Evaluating the ionospheric mass source for Jupiter's magnetosphere: An ionospheric outflow model for the auroral regions

C. J. Martin[1], L. C. Ray[1], D. A. Constable[1], D. J. Southwood[2], C. T. S. Lorch[1], M. Felici[3]

[1]Department of Physics, Lancaster University, Bailrigg, Lancaster, UK
[2]Blackett Laboratory, Imperial College London, UK
[3]Centre for Space Physics, Boston University, Boston, MA, USA

Key Points:

- An ionospheric outflow model is developed for use at Jupiter's auroral regions
- The model evaluates the effect of field-aligned currents and centrifugal forces
- A total number flux of $1.3{-}1.8\times10^{28}\,\mathrm{s}^{-1}$ is found, which is comparable to number flux from Io

Corresponding author: C. J. Martin, `c.martin1@lancaster.ac.uk`

Abstract

Ionospheric outflow is the flow of plasma initiated by a loss of equilibrium along a magnetic field line which induces an ambipolar electric field due to the separation of electrons and ions in a gravitational field and other mass dependant sources. We have developed an ionospheric outflow model using the transport equations to determine the number of particles that flow into the outer magnetosphere of Jupiter. The model ranges from 1400 km in altitude above the 1 bar level to $2.5\,\mathrm{R_J}$ along the magnetic field line and considers $\mathrm{H^+}$ and $\mathrm{H_3^+}$ as the main ion constituents. Previously, only pressure gradients and gravitational forces were considered in modelling polar wind. However, at Jupiter we need to evaluate the affect of field-aligned currents present in the auroral regions due to the breakdown of corotation in the magnetosphere, along with the centrifugal force exerted on the particles due to the fast planetary rotation rate. The total number flux from both hemispheres is found to be $1.3-1.8\times10^{28}\,\mathrm{s^{-1}}$ comparable in total number flux to the Io plasma source. The mass flux is lower due to the difference in ion species. This influx of protons from the ionosphere into the inner and middle magnetosphere needs to be included in future assessments of global flux tube dynamics and composition of the magnetosphere system.

1 Introduction

Valek et al. (2019) reported ionospheric species at high latitudes magnetically conjugate with Jupiter's inner and middle magnetosphere using the Juno spacecraft's Jovian Auroral Distributions Experiment (JADE). In this paper, we illustrate computations of the field-aligned outflow of material from the Jovian ionosphere and the ionosphere as a source of magnetospheric plasma.

The idea of ionospheric outflow as an important element of magnetospheric physics was first theorised in the terrestrial magnetosphere as a supersonic flow of charged particles from the ionosphere in the high-latitude regions of a planet (Dungey, 1961; Axford, 1968) in analogy with the solar wind supersonic flow of charged particles from the Sun. The terrestrial polar wind, comprised of H^+ and O^+, was first detected by Hoffman (1970).

Ionospheric outflow requires an imbalance of equilibrium to trigger plasma motion along the magnetic field line with low pressure at large distance. In the terrestrial case, the opening of a flux tube by reconnection at the magnetopause initiates the process and the outflow occurs on open flux tubes in the terrestrial polar cap. The first suggestion of Jovian ionospheric outflow being an important aspect of the Jovian system appears in Piddington (1969) (referenced by Kennel and Coroniti (1975)). The primary force leading to outflow was the centrifugal effect of the rapid planetary rotation on open field lines in the polar cap. However, these early predictions predate the Voyager Jupiter encounters. There is now known to be a major internal magnetospheric near-equatorial source of plasma at Io due to the moons volcanism (e.g., Hill, 1979b; Pontius Jr & Hill, 1982). Io releases $1000\,\mathrm{kg\,s^{-1}}$ of $\mathrm{SO^2}$, which forms a neutral torus around Jupiter at the radial distance of Io's orbit (5.9 R_S) (Delamere & Bagenal, 2003; Delamere et al., 2005). The neutral material is ionised, predominantly by electron impact and charge exchange, picked up and accelerated to near corotation, the angular rotation velocity of the planet (Pontius Jr & Hill, 1982; Pontius, 1995). For a thorough review of these processes, see (Thomas et al., 2004).

Estimates of the total ion particle flux emanating from near Io are in the range $(0.5-1.7)\times10^{28}$ $\mathrm{s^{-1}}$ (Bagenal, 1997) or 3×10^{28} $\mathrm{s^{-1}}$ (Saur et al., 2003). Using a model of the plasma disc, Bagenal and Delamere (2011) estimate the total ion mass flux from Io to be 260-1400 $\mathrm{kg\,s^{-1}}$. The ionised iogenic material, remaining in a plasma disc near the magnetic equator, moves outwards from the inner magnetosphere in a diffusive process. The diffusion is through a flux tube interchange motion where loaded flux tubes move away from the planet while depleted tubes (which have lost material at large distance) move back in. Beyond a radial distance of 17 R_J, the outward moving plasma begins to sub-corotate, resulting in the magnetic field (McNutt Jr et al., 1979; Bagenal et al., 2016) being bent back and the generation of field-aligned currents. Radial currents associated with the bent back field act to maintain plasma rotation (Hill, 1979a). Field-aligned currents associated with the bent back field couple the magnetosphere to the ionosphere with current closure occurring through Pedersen currents at the ionosphere. The rotation enforcement currents generate Jupiter's quasi-steady state main auroral emission (e.g., Ray et al., 2015).

The overall flux circulation providing the iogenic material diffusive transport and loss is called the Vasyliunas cycle (see e.g., Vasyliunas, 1983). In the cycle, reconnection takes place and plasma is lost through this process. The iogenic material is frozen to the magnetic field as it moves outwards but somewhere the frozen-in condition must be violated as magnetic flux has to be conserved overall but steady particle transport requires loss at large distance. The plasma loss is achieved through flux tubes undergoing magnetic reconnection in the magnetotail.

Next consider what happens to the plasma in the ionosphere in the Vasyliunas cycle. Consider a tube where the cold plasma population in ionosphere and magnetosphere are initially in equilibrium. Outward flux tube motion driven by the iogenic material near the equator will also carry ionospheric material on the flux tube to higher invariant latitude. At the same time, the volume of the tube will increase and the cold plasma pressure at high altitude on the flux tube will decrease. One can thus expect ionospheric material to move upwards to maintain equilibrium, initiating outflow. We see this as an explanation of the new Juno observations (Valek et al., 2019), which are on field lines between Ios orbit and the main auroral zone (and not on open flux as one might expect for a polar wind analogous with Earth).

A critical question is how far ionospheric plasma moves along the field during the flux tube outward motion. If the ionospheric material travels far enough along the field to participate in the reconnection, not only will some escape but the residual plasma in the equatorial region on the depleted closed tube will be a mixture of heavy iogenic material and light ionospheric plasma. The tube will move inwards and shrink in volume with the iogenic material and ionospheric material gaining energy. If the ionospheric material in the outflow induced on the outward leg of the cycle does not reach the equatorial region where reconnection takes place, ionospheric material will not be lost but also the mixing will not occur.

The purpose of this paper is to use a simple one dimensional model to examine outflow using appropriate ionospheric source conditions with varying background conditions in order to assess the nature of ionospheric flow possible on closed field lines. It is assumed that the overall magnetospheric background context in the equatorial regions is a Vasyliunas circulation system driven by diffusion of heavy material ionised in the Io torus region, as described above.

As noted earlier, at Earth the dominant plasma outflow process is in the Dungey cycle on open flux tubes. Any such process at Jupiter it is likely to be much less important to redistributing ionospheric plasma. Cowley et al. (2003) describe it at Jupiter mapping to a thin slice along the dayside and dawn flank of the magnetosphere. Indeed, some authors suggest that the Dungey-cycle does not operate at all at Jupiter (McComas et al., 2014; Delamere et al., 2005). As our motivation is to investigate mechanisms for ionospheric outflow on closed flux tubes, our context needs be the Vasyliunas cycle.

Any ionospheric outflow introduces an electric field along the background magnetic field. It is an ambipolar electric field and a direct consequence of the different masses of electrons and ions in the ionosphere. However, the Vasyliunas cycle circulation induced by the Io material sets up a global field-aligned current system (Vasyliunas, 1983) and these currents will also introduce field-aligned electric fields (Ray et al., 2010), modifying any outflow conditions. Moreover, this current system may also introduce heat through Joule heating by the associated currents in the ionosphere (e.g. Smith & Aylward, 2009); this effect could also impact the conditions for ionospheric outflow.

In contrast, the importance of ionospheric outflow as a source of plasma at Jupiter is less well understood. At both of the gas giants, an ionospheric outflow is expected to be dominated by the main ionospheric constituents, H^+ and H_3^+. Bodisch et al. (2017) discuss the relative abundance of lighter ions in Jupiter's magnetosphere during the Voyager 1 and 2 flybys. They show that protons account for up to 20% of the plasma between 5 and 30 R_J and are consistent with an ionospheric source due to a high H^+ / He^{2+} ratio (Mall et al., 1993). Further evidence comes from H_3^+ ions were also found during the Ulysses flyby (Lanzerotti et al., 1993). These results are consistent with an ionospheric particle production rate of $2\times10^{28}\,s^{-1}$ (Nagy et al., 1986).

Recently, Valek et al. (2019) observed ionospheric species at high latitudes magnetically conjugate with Jupiter's inner and middle magnetosphere using the Juno spacecraft's Jovian Auroral Distributions Experiment (JADE). The ionospheric species were found on flux tubes mainly at latitudes below the main auroral emission but poleward of the Io footprint location, a range approximately 10 degrees in latitude wide (Grodent et al., 2003). No such signatures of ionospheric plasma were found at polar latitudes.

At Saturn, mid-latitude ionospheric outflow has also been detected. (Felici et al., 2016) presented evidence of outflow at 36 R_S (1 R_S = 60,268 km) in the tail region (2200 Saturn local time) using the Cassini spacecraft. The authors estimate that this outflow event shows a number flux of between (6.1-2.9) $\times10^{27}$ and (2.9-1.4)$\times10^{28}\,s^{-1}$, corresponding to a total mass source of (10 ± 4) to (49 ± 23) $kg\,s^{-1}$, numbers comparable to the mass source from the moon Enceladus (60-100 $kg\,s^{-1}$) (Fleshman et al., 2013).

These initial observations of ionospheric outflow at Jupiter and Saturn are enticing, as the changes to the magnetospheric plasma composition and energy have consequences for magnetospheric dynamics. A better understanding of the drivers of ionospheric outflow at the giant planets requires modelling similar to the extensive efforts applied at the terrestrial system (see review by Lemaire et al. (2007)). Based on Juno observations (Valek et al., 2019), ionospheric outflow may contribute to the composition of magnetospheric plasma near the auroral zone boundary i.e. in the middle magnetosphere.

The goal of this study is to describe ionospheric outflow at Jupiter, including the effects of centrifugal forces due to the rapid planetary rotation rate and field-aligned auroral currents from the coupling of the magnetosphere and the ionosphere. Section 2 describes the model, which uses a hydrodynamic approach. Section 3 evaluates ionospheric outflow at Jupiter over a range of initial conditions appropriate to the system. The implications of the ionospheric contribution to Jupiter's magnetosphere are discussed Section 4 with a summary of our analysis presented in Section 5.

2 Model

The outflow model described here is a hydrodynamic, multi-fluid, 1-D model. The spatial dimension is along the magnetic field, which has a cross-sectional area, A, that increases as the reciprocal of the field strength. The model introduces contributions from gravitational forces, centrifugal forces, pressure gradients and forces associated with the ambipolar electric field. As we are expanding the model to a number of planetary radii, the JRM09 magnetic field model (Connerney et al., 2018) is implemented to estimate the flux tube cross-section.

The two major ion species, H^+ and H_3^+, are evaluated through use of the five-moment gyrotropic transport equations (Banks & Kockarts, 1973) which are based on the continuity of mass (equation 1), momentum (equation 2) and energy (equation 3) in a system. The equations also include the centrifugal acceleration term ($\omega^2 r$), where ω is the angular velocity due to corotation and r is cylindrical distance from the rotational axis resolved along the field line. Only rigid corotation is evaluated.

$$\frac{\partial}{\partial t}(A\rho_i) = -\frac{\partial}{\partial r}(A\rho_i u_i) + AS_i \tag{1}$$

$$\frac{\partial}{\partial t}(A\rho_i u_i) = -\frac{\partial}{\partial r}(A\rho_i u_i^2) - A\frac{\partial P_i}{\partial r} + A\rho_i\left(\frac{e}{m_i}E_\parallel - g + \omega^2 r\right) + \frac{DM_i}{Dt} + Au_iS_i \tag{2}$$

$$\frac{\partial}{\partial t}(\frac{1}{2}A\rho_i u_i^2 + AP_i\frac{1}{\gamma_i - 1}) = -\frac{\partial}{\partial r}(\frac{1}{2}A\rho_i u_i^3 - Au_iP_i\frac{\gamma_i}{\gamma_i - 1}) + Au_i\rho_i\left(\frac{e}{m_i}E_\parallel - g + \omega^2 r\right) + \frac{\partial}{\partial r}\left(A\kappa_i\frac{\partial T_i}{\partial r}\right) + \frac{DM_i}{Dt} + \frac{DE_i}{Dt} + \frac{1}{2}Au_i^2S_i \tag{3}$$

A subscript of $'i'$ denotes this is done for each ionic species separately, ρ is mass density, u is velocity, S is the mass production rate, P is pressure, e is electron charge, m is the mass of the ion species, g is the gravitational acceleration, κ is the thermal conductivity, T is temperature, and γ is the specific heat ratio. $\frac{DM_i}{Dt}$ is the rate of momentum exchange and $\frac{DE_i}{Dt}$ is the rate of energy exchange.

We assume $\kappa_i = 4.6\times10^6 \frac{m_i}{m_p}^{-0.5}T^{5/2}e\,\mathrm{Jm^{-1}s^{-1}K^{-1}}$ and $\kappa_e = 1.8\times10^8T^{5/2}e\,\mathrm{Jm^{-1}s^{-1}K^{-1}}$ (Banks & Kockarts, 1973), where m_p is the proton mass. $\frac{\partial}{\partial r}\left(A\kappa_i\frac{\partial T_i}{\partial r}\right)$ is considered negligible in this formulation. This is determined by magnitude analysis at the first iterations (<0.5% magnitude compared to the largest terms in equation 3). The full term is removed to improve computational efficiency.

The magnetic-field-aligned components of the gravitational and centrifugal acceleration terms are evaluated along the field line. The parallel electric field, $E_\parallel$, produced by the net charge separation is given by:

$$E_\parallel = -\frac{1}{en_e}\left(\frac{\partial}{\partial r}(P_e - \rho_e u_e^2) + \frac{\frac{dA}{dr}}{A}\rho_e u_e^2\right) + \frac{1}{en_e}\frac{\partial}{\partial r}\left(\sum_i \frac{m_e}{m_i}\left((u_e - u_i)S_i - \frac{DM_i}{Dt}\right) + \frac{DM_e}{Dt}\right) \tag{4}$$

A subscript of $'e'$ denotes the quantity for an electron and n is the number density. The remaining unknowns are $\frac{DM_i}{Dt}$ (rate of momentum exchange) and $\frac{DE_i}{Dt}$ (rate of energy exchange) which are given by:

$$\frac{DM_i}{Dt} = -\sum_y \rho_i\nu_{ij}(u_i - u_y) \tag{5}$$

$$\frac{DE_i}{Dt} = \sum_y \frac{\rho_i\nu_{iy}}{m_i + m_y}\left(3k_b(T_y - T_i) + m_j(u_i - u_y)^2\right) \tag{6}$$

A subscript of $'y'$ denotes the different neutral species, ν_{iy} is the collision frequency between the ionic species and neutral species, k_b is the Boltzmann constant. We assume the neutral atmosphere is at rest (u_y =0). The momentum exchange rate for electrons $\frac{\delta M_e}{\delta t}$ is considered negligible compared to the dominant electron pressure gradient in equation 4.

We use charge neutrality for singly ionised species (7) and a steady state electron velocity assumption (8) to solve for the density and velocity of the electrons. To solve for the energy of the electrons we use an energy equation (9).

$$n_e = \sum_i n_i \tag{7}$$

$$u_e = \frac{1}{n_e}\left(\sum_i n_i u_i - \frac{j}{e}\right) \tag{8}$$

$$\begin{aligned}\rho_e \frac{\partial T_e}{\partial t} &= -\rho_e u_e \frac{\partial T_e}{\partial r} - T_e\left(S_e + \frac{\gamma_e - 1}{A}\rho_e \frac{\partial}{\partial r}(A u_e)\right) \\ &+(\gamma_e - 1)\frac{m_e}{k_b}\frac{DE_e}{Dt} + (\gamma_e - 1)\frac{m_e}{k_b A}\frac{\partial}{\partial r}\left(A\kappa_e \frac{\partial T_e}{\partial r}\right)\end{aligned} \tag{9}$$

$\frac{DE_e}{Dt}$ and $\frac{\partial}{\partial r}\left(A\kappa_e \frac{\partial T_e}{\partial r}\right)$ are negligible compared to the other terms so the final two terms are not used. j is current density of field-aligned currents which is scaled using the flux tube cross-section $j = j_0 A_0/A$ where j_0 is is the current density at a reference altitude A_0. The current density profile as a function of latitude (Ray et al., 2015) is applied at a height of 1000 km, coincident with the peak in ionospheric electron density.

The temporal resolution is 0.01 s. The field line is split into 75 km wide spatial grid points, which relates to 2400 grid points for a field line of length 2.5 R_J over which the spatial derivatives are estimated using central difference Euler for first order derivatives. This method is used as the terms are not stiff when using a time step of 0.01 s or less. We note that the results are robust for smaller spatial grid sizes (down to 20 km) and as such we use 75 km for efficiency in computing.

Initial distributions are specified along the entire spatial domain, and are derived from either the initial temperature distribution or the initial density distribution using the following formulations. Velocity is found from equating the thermal energy to the kinetic energy, $u_i = \sqrt{\frac{2k_b T_i}{m_i}}$. Mass production is estimated as a 1% fraction of the mass density, and the results are robust against a 2 order of magnitude change in this value. Pressure is calculated from the plasma pressure equation, $P_i = n_i k_b T_i$.

The neutral species evaluated within the model are H_2, He and H. Each species is used to calculate the mass and energy exchange rates which require a collision frequency which is calculated using:

$$\nu_{iy} = 2.21\pi \frac{\rho_y}{m_i + m_y}\frac{\lambda_y e^2}{\frac{m_i m_y}{m_i + m_y}}, \tag{10}$$

where λ_y is the neutral gas polarisability which are $0.82 \times 10^{-30}\,\mathrm{m}^3$, $0.21 \times 10^{-30}\,\mathrm{m}^3$ and $0.67 \times 10^{-30}\,\mathrm{m}^3$ for H_2, He and H respectively (Schunk & Nagy, 2000). Initial values of density of the ionic and neutral species are extrapolated with an exponential decay, with appropriate scale height, from 1400 km in 'JIM'- the Jovian Ionospheric Model (Achilleos et al., 1998). An initial distribution of temperature is also retrieved from the Jovian Ionospheric Model which increases as an exponential to 0.5 R_J and then is estimated by a logarithmic decay to a base value. Evaluation and robustness of these values is discussed later. All initial value are shown in figure 1, along with the flux tube cross-sectional area, A. The model is run until quasi-steady-state is reached, or until the difference between two iterations is negligible (difference between outputs of two iterations is < 0.1% for 1 second in simulation time, or 100 time steps). Number flux along a single flux rope is calculated as $n_e u_e$ multiplied by the cross-sectional area A. This can also be calculated for each ionic species.

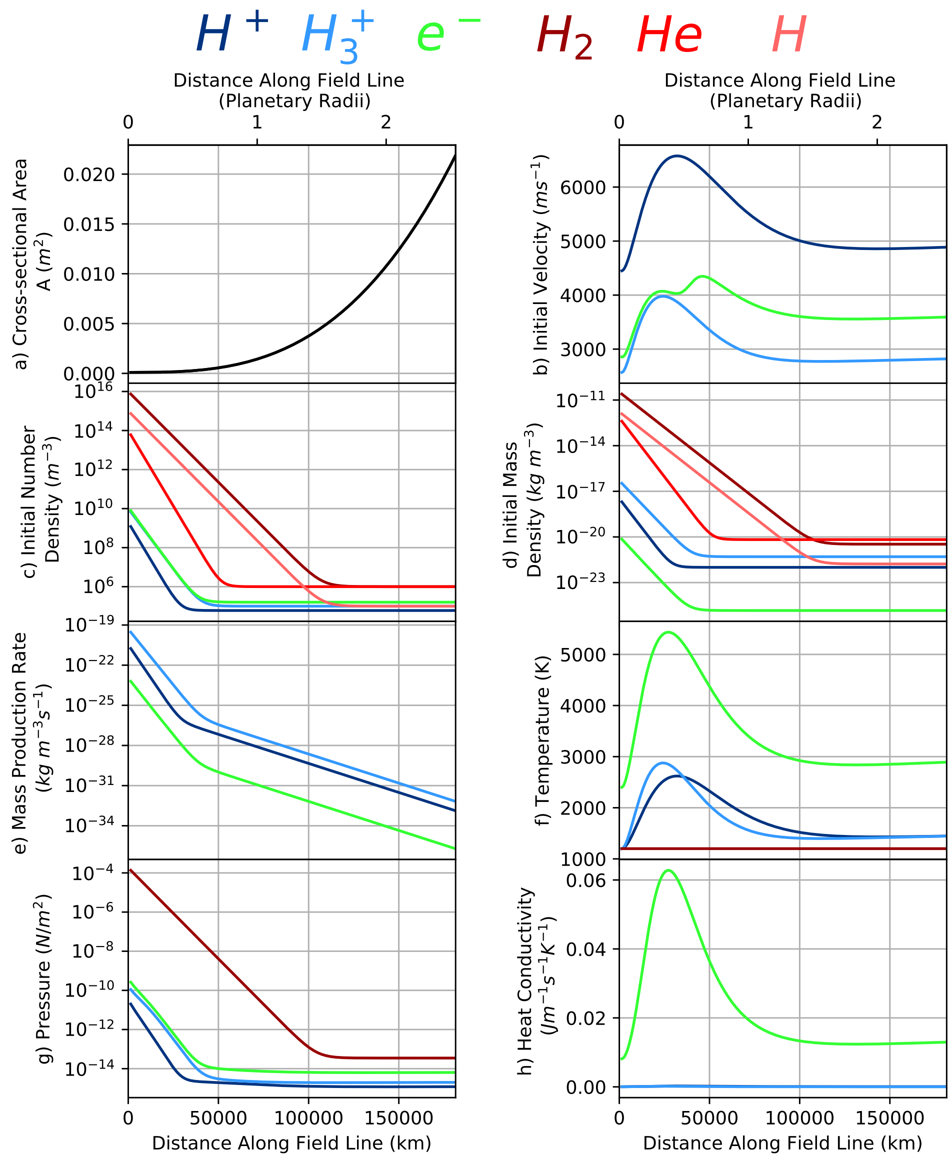

Figure 1. Initial conditions a) cross-sectional area of flux rope, b) velocity of ions and electrons. Neutral velocity is $0\,\mathrm{kms^{-1}}$, c) number density of ions, electrons and neutrals, d) mass density of ions, electrons and neutrals, e) mass production rate of ions and electrons, f) temperature profile of ions, electrons and neutrals (neutrals all have the same temperature), g) pressure of ions, electrons and neutrals (neutrals all have the same pressure), h) thermal conductivity of ions and electrons, for the ionospheric outflow model along a field line from 1400 km to $2.5\,\mathrm{R_J}$ from the 1 bar level. Ions are shown in blue, electrons in green and neutrals in red. The key to the different colours is at the top of the figure.

3 Results

Figure 2 displays the quasi-steady-state parallel electric field, the acceleration terms (gravitational, centrifugal, electric field), and electron and ion fluxes, corresponding to an initial values described as 'run 1' in table 1. The electric field (figure 2a) peaks around 10000 km along the field line, which is the position at which the separation of the electrons and ions is largest due to the corresponding densities and temperatures. The electric field then reduces to a steady value. This pattern is followed by the acceleration due to the electric field in both the H^+ and H_3^+ ions (dark blue and light blue solid curves in 2b).

Additionally, we see the gravitational acceleration decreases with radial distance along the field line, whilst the centrifugal force increases (dashed teal and dashed purple in figure 2b). At around $2\,R_J$ the centrifugal acceleration becomes dominant over the gravitational acceleration. A density depletion is expected to occur in this region.

The total particle source from the auroral oval can be estimated by multiplying the number flux of particles with the area of a 2° wide oval at 75°−77° latitude around the planet, and then multiplying by 2 to give a value for both hemispheres. This is done at an altitude of 25,000 km, where the number flux becomes approximately constant. The initial conditions described for figure 2, and the total particle and mass sources (calculated by taking the relative proportions of electrons, H^+ and H_3^+) are shown by 'run 1' in table 1. A field-aligned current function (Ray et al., 2015) is used where the largest magnitude current used is $3 \times 10^{-6}\,\mathrm{Am}^{-2}$ scaled from the bottom of the ionosphere.

However, we note that the density and temperature in the ionosphere may vary significantly, and the upward field-aligned currents alone may range from 1-7 $\mu\mathrm{Am}^{-2}$ (Ray et al., 2009). As such, we vary the field-aligned currents, temperature, and number densities of n_{H^+} and $n_{H_3^+}$ to present a range of total particle and mass source rates. The extremes of these ranges are presented in table 1 as 'run 2' and 'run 3', where 'run 3' represents a more auroral-like ionosphere, and 'run 2' represents a more non-auroral ionosphere. This results in a range for the total particle source of 2.4 - 4.9 $\times 10^{27}\,\mathrm{s}^{-1}$, and a range in the total mass source of 4.3 - 8.5 $\mathrm{kg\,s}^{-1}$. As the ranges of number density and temperature used to evaluate an uncertainty are large, we assume this is the largest source of uncertainty in the model and do not evaluate the intrinsic errors involved with the numerical methods used.

By mapping the ionosphere out to the magnetically conjugate area in the equatorial region (Vogt et al., 2011), the particle and mass flux that reaches the equatorial region can be quantified. We use flux equivalence, $A_I F_I = A_E F_E$, where A_I is the area in the ionosphere, and F_I is the flux through this area. A_E is the area in the equatorial region that the ionospheric area maps to, and F_E is the flux through the equatorial area. We then run the model over the auroral region at 75° to 77° in steps of 0.02°, where a upward current is present between 75° - 76° and a downward current is present between 76° to 77°. The strength and direction of the field-aligned currents in this region follow the model in figure 9f of Ray et al. (2015). Figure 3 shows the electron, ion and mass flux scaled to the equator from a height of 25,000 km. The electron flux is highly modified by the field-aligned currents present, where it is enhanced by a downward current and retarded by an upward current in the auroral regions. Electron flux resulting from the inclusion of FACs is shown as the solid green curve, the dotted green curve shows electron flux with FACs omitted.

We extend figure 3 to include the equator-ward range of latitudes of 65-75° using a dipole field to map the field lines to the equator between 5-15 R_J, shown in figure 4. This is the region bounded by the Io footprint and the auroral oval described by Valek et al. (2019). The model implements no field-aligned currents in this area, and a gen-

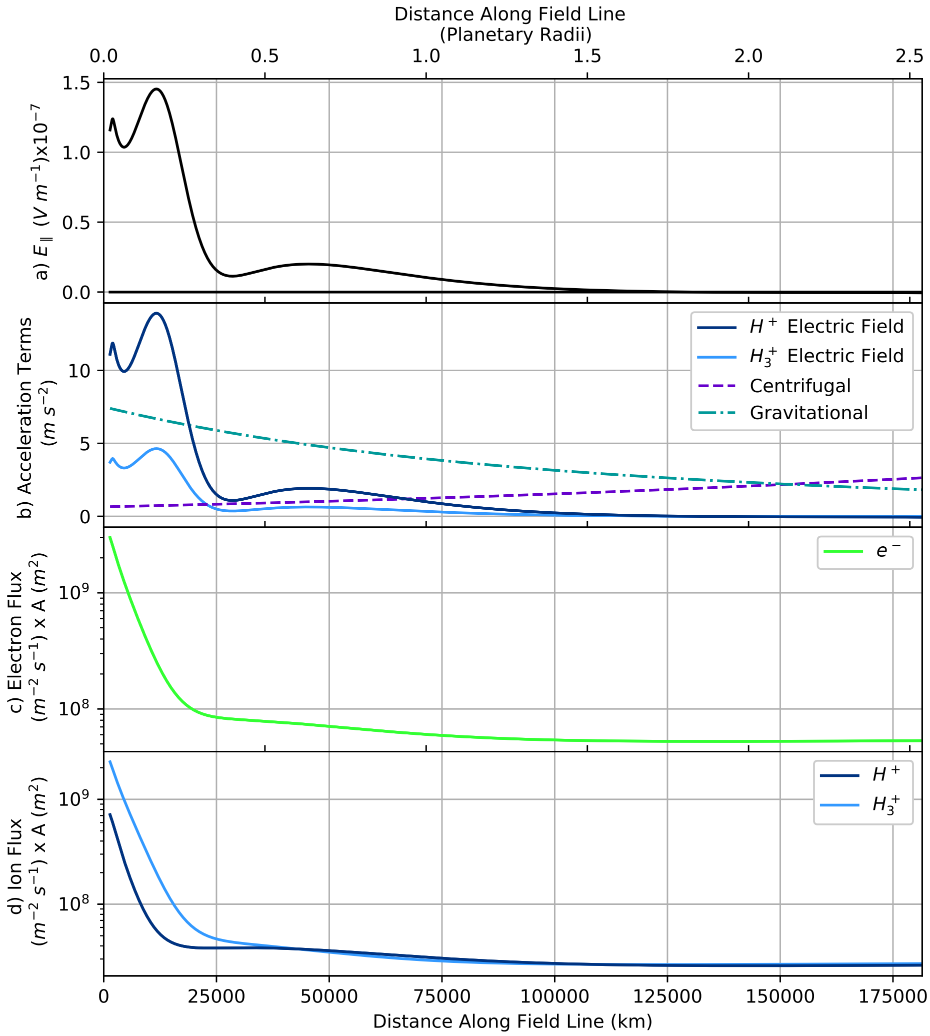

Figure 2. Results for 'run 1' of the ionospheric outflow model, where initial values are T = 700 K, $n_{H+} = 2 \times 10^9\,\mathrm{m}^{-3}$ and $n_{H_3^+} = 1 \times 10^{10}\,\mathrm{m}^{-3}$ for the ionospheric end of the flux tube. a) Shows the electric field from 1400 km to 2.5 R_J in altitude, b) shows the magnitude of the acceleration terms, where solid dark blue is due to the electric field acting on the H^+ ions, solid pale blue is due to the electric field acting on the H_3^+ ions, the purple dashed line is the centrifugal acceleration, and the dot-dash teal line is the gravitational acceleration, c) shows the electron flux, scaled to the cross sectional-area and d) shows the ion fluxes scaled to the cross sectional-area, where dark blue is H^+ ions and pale blue is H_3^+ ions.

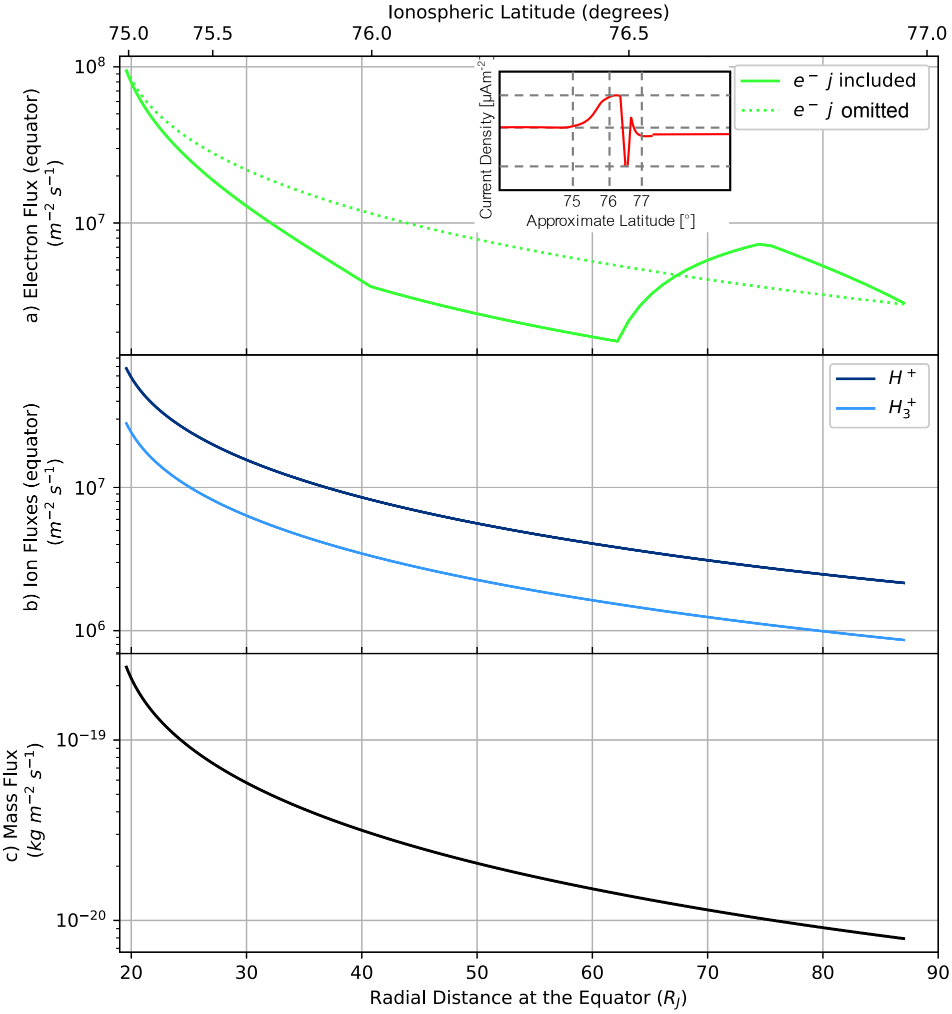

Figure 3. An example of results for the mapping of the ionospheric outflow to the equator, where initial values in this example are T = 700 K, $n_{H+} = 2 \times 10^{10}\,\mathrm{m}^{-3}$ and $n_{H_3^+} = 1 \times 10^{9}\,\mathrm{m}^{-3}$ for the ionospheric end of the flux tube, a) shows the electron flux, solid green is with field-aligned currents, dotted green is without field-aligned currents for reference, where the insert in a) shows the shape of the field-aligned currents. b) Shows the ion fluxes, where solid dark blue is H^+ ions, solid pale blue is H_3^+ ions, c) shows the mass flux. This example is for auroral field lines which are mapped to the equator using the Vogt et al. (2011) mapping.

Table 1. Comparison of five model runs over an area of specified 'oval size' in degrees wide to show the large variation in particle and mass source rates. Run 3 has auroral-like values with high temperature and low densities at the ionospheric end of the field line, run 2 has non-auroral region values with low temperatures and high densities at the ionospheric end of the field line. Values for run 1 correspond to the results presented in figure 2, run 4 shows an example of the same initial conditions as run 1 but excluding both field-aligned currents and centrifugal force. Run 5 shows an example of a run for the sub-auroral regions.

Input Variables at Ionosphere	Run 1 Figure 2	Run 2 Non Auroral	Run 3 Auroral	Run 4 Exc. FAC	Run 5 Sub Auroral
n_{H^+} [m^{-3}]	2×10^9	5×10^8	1×10^{10}	2×10^9	2×10^9
$n_{H_3^+}$ [m^{-3}]	1×10^{10}	1×10^9	5×10^{10}	1×10^{10}	1×10^{10}
T [K]	700	200	2000	700	200
j (peak value) [μA m^{-2}]	3	0	7	0	0
Oval size (°)	2	2	2	2	10
Output Variables					
Total particle source rate [s^{-1}]	3.2×10^{27}	2.4×10^{27}	4.9×10^{27}	1.9×10^{27}	1.2×10^{28}
Total mass source rate [kg s^{-1}]	7.4	4.3	8.5	3.9	18.4

eral trend of decreasing particle flux is found due to the increasing area of which each ionospheric area maps out to the equator.

Combined with the 2° wide auroral region we discussed above, a total particle source from polar wind at Jupiter would be between $1.3-1.8\times10^{28}\,s^{-1}$ and a mass source of 18.7 - 31.7 kg s^{-1}. This is a comparable number source, but a much smaller mass source than that of Io. This total mass source is also within the range of total mass sources from the solar wind discussed earlier (20 and 150 kg s^{-1}).

4 Discussion

While our model is spatially 1D, compounding where and under what conditions the model is run, we can describe the behaviour of ionospheric outflow in Jupiter's polar regions by applying it for a range of latitudes and auroral current conditions. Figure 3 displays the results of 100 runs of the model along one line of longitude ($\sim$ 0300 local time) between latitudes of 75-77°. This is done to estimate the effects of field-aligned currents on the flux that will reach the equator along each of these field lines, assuming that this latitude region is where the auroral oval at Jupiter is found. The current-latitude relationship from Ray et al. (2015) is used, and it is clear that an inverse relation is present between current and electron flux at the equator.

The latitudinal structure of the auroral currents has consequences for the total ionospheric outflow. The region of upward current causes the electron flux (solid green curve) to reduce in this area, and the region of downward current causes the electron flux to increase. This effect is due to the fact that electrons are already moving along the field line in either the opposite (upward current) direction, and as such decreases the number of electrons moving outward, or outward along the field line (downward current) and as such increases the number of electrons moving outward. The dotted green curve shows the relation without field-aligned currents. This relationship is dominated by the gen-

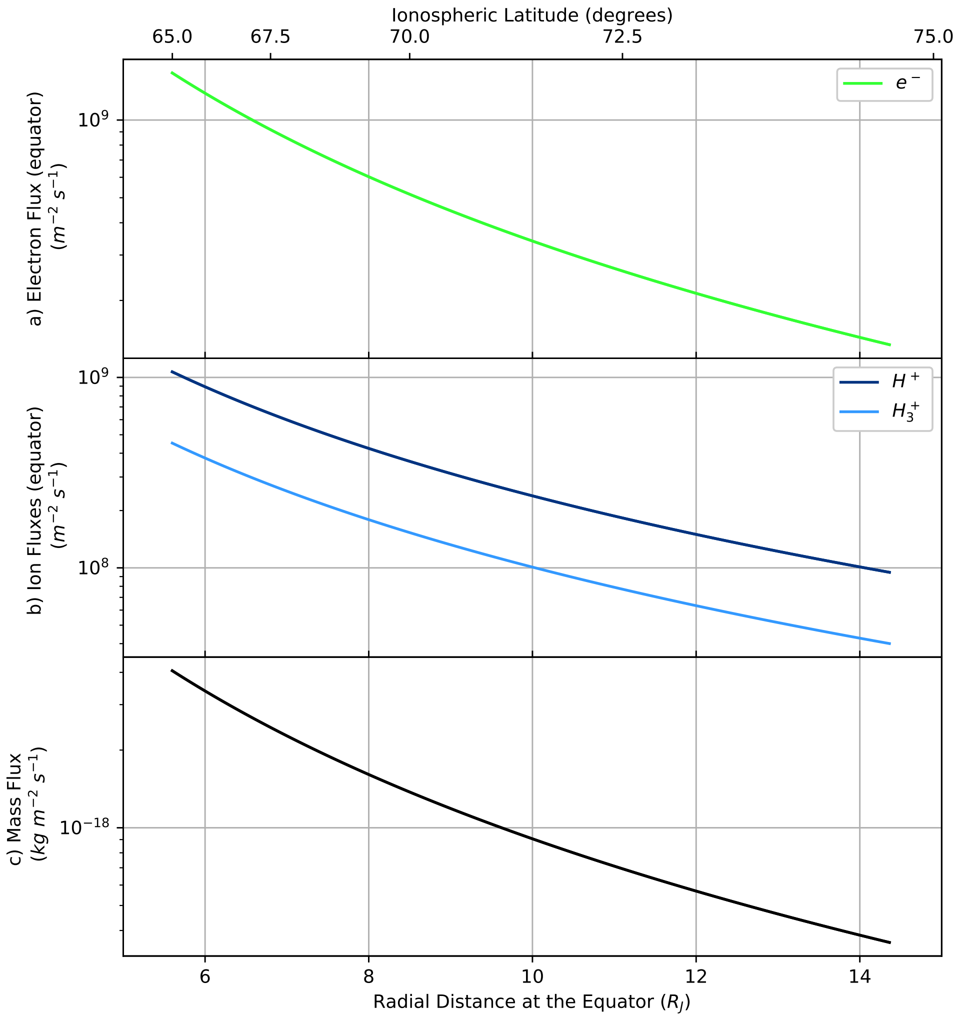

Figure 4. An example of results for the mapping of the ionospheric outflow to the equator, where initial values in this example are T = 700 K, $n_{\mathrm{H}+} = 2 \times 10^{10}\,\mathrm{m}^{-3}$ and $n_{\mathrm{H}_3^+} = 1 \times 10^{9}\,\mathrm{m}^{-3}$ for the ionospheric end of the flux tube. a) Shows the electron flux, b) shows the ion fluxes, where solid dark blue is H^+ ions, solid pale blue is H_3^+ ions, and c) shows the mass flux. This example is for sub-auroral field lines which are mapped to the equator using a dipole field model.

eral decrease with increasing latitude which is due to the area that each latitude is mapping out to increases at the equator.

We note that very little effect is seen in the ion flux and the mass flux due to the much smaller mass of the electrons. Hence, downward field-aligned currents increase the overall ionospheric outflow and upward field-aligned currents decrease the overall ionospheric outflow. Spatial and temporal changes in field-aligned currents are not investigated at this time. However, discussion of their effects with regard to Saturn can be found in the companion manuscript, Martin et al. (Accepted).

In addition to the field-aligned currents, this model also takes into account the effects of centrifugal acceleration. As shown in figure 2b, the centrifugal acceleration (purple dashed line) increases in magnitude along the spatial domain of the model, where at around 150,000 km it becomes dominant over the gravitational acceleration. However, it has a non-zero contribution to the velocity of the particles flowing from the ionosphere. Run 4 in table 1 excludes both the centrifugal force and field-aligned currents. As a result, the total particle source over a 2° oval at the polar region is reduced by a near factor of 2 from the range of values given when the centrifugal force is included. Thus, we conclude that the centrifugal force acts to enhance the flux of particles from the ionosphere at the giant planets.

The results from Valek et al. (2019) show an increased value of ionospheric outflow between the Io footprint and the auroral oval on average. If we assume that ionospheric outflow occurs only at latitudes between the Io footprint and the auroral oval, which is approximately 10° in latitude wide (Grodent et al., 2003), we find a total particle source of $1.3{-}1.8{\times}10^{28}\,\mathrm{s}^{-1}$ which equates to a total mass source of 14.4 - 23.2 $\mathrm{kg\,s}^{-1}$, an example of which is shown in 'run 5' of table 1. This range is calculated using the same ranges of input values for runs 1 and 2, with no field-aligned currents as described for this region by Ray et al. (2015). Changes in ionospheric density over this region could be included in future development of this model to give a more accurate representation of the flux reaching the equator along the field lines. For the time being, a constant density is used which leads to the smooth decrease in the fluxes. Valek et al. (2019) also showed that very little ionospheric plasma is found on polar cap field lines. This may indicate that the Dungey cycle does not efficiently drive ionospheric outflow at Jupiter, if the cycle is present at all.

A complete picture of the sources of Jovian magnetospheric plasma will also requires eventual understanding of the entry and assimilation of solar wind material as the estimates based on incident flux by (Hill et al., 1983) and (Bagenal & Delamere, 2011) make clear.

5 Summary

An ionospheric outflow model was developed to model the outflow at the auroral regions of Jupiter. The model uses the 5-moment gyrotropic transport equations, along with the assumption of quasi-neutrality and a steady state electron velocity. The effects of field-aligned currents in the auroral region and the centrifugal acceleration experienced by the particles are included. The main conclusions of the study are:

1. A total particle source for both hemispheres is found to be $1.3 - 1.8 \times 10^{28}\,\mathrm{s}^{-1}$ when considering the auroral and sub-auroral source regions.
2. This corresponds to a total mass source of 18.7 - 31.7 $\mathrm{kg\,s}^{-1}$.
3. These values are comparable to studies of Io as a source (Bagenal, 1997; Saur et al., 2003) and is close to estimates of ionospheric particle production rate by Nagy et al. (1986).

4. The total ionic mass source from Io is far larger than the ionic mass source of the ionosphere found in this study, where at Io the major ion is assumed to be SO_2^+ compared to the ionospheric H^+ and H_3^+ ions.
5. Centrifugal force and downward field-aligned currents act to increase the flow of electrons from the polar regions, whereas upward field-aligned currents act to decrease the flow of electrons from the ionosphere.
6. Mapping the flux from the auroral region to the equator, we find a radially dependent mass flux with a near exponential decrease from the middle magnetosphere to the outer, with a electron flux which is highly modulated by the field-aligned currents present.

Constraints on initial conditions to improve a future model and give local time and latitudinal variation may be possible with the Juno spacecraft now in a position to measure ionospheric outflow and plasma properties in the high latitudes at Jupiter.

Acknowledgments

CJM, LCR and DAC were funded by STFC grant number ST/R000816/1. CTSL was funded by a STFC studentship. Work by DJS at Imperial College was supported by STFC grant ST/N000692/1. CJM acknowledges Sarah Badman, Joe Kinrade, Alex Bader and Rebecca Gray for informative discussion and Nick Achilleos for discussion and information pertaining to the Jovian Ionospheric Model . CJM acknowledges the Europlanet 2020 RI project for funding to attend the Europlanet NA1 workshop: Uniting Planetary Modelling and Data Analysis. The ionospheric outflow model is available on request from CJM and LCR and model outputs are available from a Lancaster University repository with DOI number 10.17635/lancaster/researchdata/312.

References

Achilleos, N., Miller, S., Tennyson, J., Aylward, A., Mueller-Wodarg, I., & Rees, D. (1998). JIM: A time-dependent, three-dimensional model of Jupiter's thermosphere and ionosphere. *Journal of Geophysical Research: Planets*, *103*(E9), 20089–20112. doi: 10.1029/98JE00947

Axford, W. I. (1968). The polar wind and the terrestrial helium budget. *Journal of Geophysical Research*, *73*(21), 6855–6859. doi: 10.1029/JA073i021p06855

Bagenal, F. (1997). The ionization source near Io from Galileo wake data. *Geophysical research letters*, *24*(17), 2111–2114. doi: 10.1029/97GL02052

Bagenal, F., & Delamere, P. A. (2011). Flow of mass and energy in the magnetospheres of Jupiter and Saturn. *Journal of Geophysical Research: Space Physics*, *116*(A5). doi: 10.1029/2010JA016294

Bagenal, F., Wilson, R. J., Siler, S., Paterson, W. R., & Kurth, W. S. (2016). Survey of Galileo plasma observations in Jupiter's plasma sheet. *Journal of Geophysical Research: Planets*, *121*(5), 871–894. doi: 10.1002/2016JE005009

Banks, P. M., & Kockarts, G. (1973). *Aeronomy.* Academic Press.

Bodisch, K. M., Dougherty, L. P., & Bagenal, F. (2017). Survey of Voyager plasma science ions at Jupiter: 3. Protons and minor ions. *Journal of Geophysical Research: Space Physics*, *122*(8), 8277–8294. doi: 10.1002/2017JA024148

Connerney, J. E. P., Kotsiaros, S., Oliversen, R. J., Espley, J. R., Jørgensen, J. L., Joergensen, P. S., ... Levin, S. M. (2018). A new model of Jupiter's magnetic field from Juno's first nine orbits. *Geophysical Research Letters*, *45*(6), 2590–2596. doi: 10.1002/2018GL077312

Cowley, S. W. H., Bunce, E. J., Stallard, T. S., & Miller, S. (2003). Jupiter's polar ionospheric flows: Theoretical interpretation. *Geophysical research letters*, *30*(5). doi: 10.1029/2002GL016030

Delamere, P. A., & Bagenal, F. (2003). Modeling variability of plasma conditions in the Io torus. *Journal of Geophysical Research: Space Physics*, *108*(A7). doi: 10.1029/2002JA009706

Delamere, P. A., Bagenal, F., & Steffl, A. (2005). Radial variations in the Io plasma torus during the Cassini era. *Journal of Geophysical Research: Space Physics*, *110*(A12). doi: 10.1029/2005JA011251

Dungey, J. W. (1961). Interplanetary magnetic field and the auroral zones. *Physical Review Letters*, *6*(2), 47. doi: 10.1103/PhysRevLett.6.47

Felici, M., Arridge, C. S., Coates, A. J., Badman, S. V., Dougherty, M. K., Jackman, C. M., ... Sergis, N. (2016). Cassini observations of ionospheric plasma in Saturn's magnetotail lobes. *Journal of Geophysical Research: Space Physics*, *121*(1), 338–357. doi: 10.1002/2015JA021648

Fleshman, B. L., Delamere, P. A., Bagenal, F., & Cassidy, T. (2013). A 1-D model of physical chemistry in Saturn's inner magnetosphere. *Journal of Geophysical Research: Planets*, *118*(8), 1567–1581. doi: 10.1002/jgre.20106

Grodent, D., Clarke, J. T., Kim, J., Waite Jr, J. H., & Cowley, S. W. H. (2003). Jupiter's main auroral oval observed with HST-STIS. *Journal of Geophysical Research: Space Physics*, *108*(A11). doi: 10.1029/2003JA009921

Hill, T. W. (1979a). Inertial limit on corotation. *Journal of Geophysical Research: Space Physics*, *84*(A11), 6554–6558. doi: 10.1029/JA084iA11p06554

Hill, T. W. (1979b). Rates of mass, momentum, and energy transfer at the magnetopause. In *Magnetospheric boundary layers* (Vol. 148).

Hill, T. W., Dessler, A. J., & Goertz, C. K. (1983). Magnetospheric models. *Physics of the Jovian magnetosphere*, 353–394. doi: 10.1017/CBO9780511564574.012

Hoffman, J. H. (1970). Studies of the composition of the ionosphere with a magnetic deflection mass spectrometer. *International Journal of Mass Spectrometry and Ion Physics*, *4*(4), 315–322. doi: 10.1016/0020-7381(70)85047-1

Kennel, C. F., & Coroniti, F. V. (1975). Is jupiter's magnetosphere like a pulsar's or earth's? In *The magnetospheres of the earth and jupiter* (p. 451-477). Springer. doi: /10.1007/978-94-010-1789-3_36

Lanzerotti, L. J., Maclennan, C. G., & Feldman, D. M. (1993). Ulysses measurements of energetic H_3 molecules in Jupiter's magnetosphere. *Journal of Geophysical Research: Space Physics*, *98*(A12), 21145–21149. doi: 10.1029/93JA02589

Lemaire, J. F., Peterson, W. K., Chang, T., Schunk, R. W., Barakat, A. R., Demars, H. G., & Khazanov, G. V. (2007). History of kinetic polar wind models and early observations. *Journal of Atmospheric and Solar-Terrestrial Physics*, *69*(16), 1901–1935. doi: 10.1016/j.jastp.2007.08.011

Mall, U., Geiss, J., Balsiger, H., Gloeckler, G., Galvin, A., & Wilken, B. (1993). Hydrogen from Jupiter's atmosphere in the Jovian magnetosphere. *Planetary and space science*, *41*(11-12), 947–951. doi: 10.1016/0032-0633(93)90099-N

Martin, C. J., Ray, L. C., Felici, M., Constable, D. A., Lorch, C. T. S., Kinrade, J., & L, G. R. (Accepted). The effect of field-aligned currents and centrifugal forces on ionospheric outflow at Saturn. *Journal of Geophysical Research: Space Physics*.

McComas, D., Bagenal, F., & Ebert, R. (2014). Bimodal size of Jupiter's magnetosphere. *Journal of Geophysical Research: Space Physics*, *119*(3), 1523–1529. doi: 10.1002/2013JA019660

McNutt Jr, R. L., Belcher, J. W., Sullivan, J. D., Bagenal, F., & Bridge, H. S. (1979). Departure from rigid co-rotation of plasma in Jupiter's dayside magnetosphere. *Nature*, *280*, 803. doi: 10.1038/280803a0

Nagy, A., Barakat, A., & Schunk, R. (1986). Is Jupiter's ionosphere a significant plasma source for its magnetosphere? *Journal of Geophysical Research: Space Physics*, *91*(A1), 351–354. doi: 10.1029/JA091iA01p00351

Piddington, J. H. (1969). *Cosmic Electrodynamics.*

Pontius, D. H. (1995). Implications of variable mass loading in the Io torus: The

Jovian flywheel. *Journal of Geophysical Research: Space Physics*, *100*(A10), 19531–19539. doi: 10.1029/95JA01554

Pontius Jr, D. H., & Hill, T. W. (1982). Departure from corotation of the Io plasma torus: Local plasma production. *Geophysical Research Letters*, *9*(12), 1321–1324. doi: 10.1029/GL009i012p01321

Ray, L. C., Achilleos, N. A., & Yates, J. N. (2015). The effect of including field-aligned potentials in the coupling between Jupiter's thermosphere, ionosphere, and magnetosphere. *Journal of Geophysical Research: Space Physics*, *120*(8), 6987–7005. doi: 10.1002/2015JA021319

Ray, L. C., Ergun, R. E., Delamere, P. A., & Bagenal, F. (2010, September). Magnetosphere-ionosphere coupling at Jupiter: Effect of field-aligned potentials on angular momentum transport. *J. Geophys. Res.*, *115*, A09211. doi: 10.1029/2010JA015423

Ray, L. C., Su, Y.-J., Ergun, R. E., Delamere, P. A., & Bagenal, F. (2009). Current-voltage relation of a centrifugally confined plasma. *Journal of Geophysical Research: Space Physics*, *114*(A4). doi: 10.1029/2008JA013969

Saur, J., Strobel, D. F., Neubauer, F. M., & Summers, M. E. (2003). The ion mass loading rate at Io. *Icarus*, *163*(2), 456–468. doi: 10.1016/S0019-1035(03)00085-X

Schunk, R. W., & Nagy, A. F. (2000). Ionospheres. *Plasma Physics, and Chemistry, Cambridge University Press*.

Smith, C. G. A., & Aylward, A. D. (2009, January). Coupled rotational dynamics of Jupiter's thermosphere and magnetosphere. *Annales Geophysicae*, *27*, 199-230.

Thomas, N., Bagenal, F., Hill, T., & Wilson, J. (2004). The Io neutral clouds and plasma torus. *Jupiter. The planet, satellites and magnetosphere*, *1*, 561–591.

Valek, P. W., Allegrini, F., Bagenal, F., Bolton, S. J., Connerney, J. E. P., Ebert, R. W., … Wilson, R. J. (2019). Jovian High-Latitude Ionospheric Ions: Juno In Situ Observations. *Geophysical Research Letters*, *46*. doi: 10.1029/2019GL084146

Vasyliunas, V. M. (1983). Physics of the Jovian magnetosphere. *Plasma distribution and flow*, 395–453.

Vogt, M. F., Kivelson, M. G., Khurana, K. K., Walker, R. J., Bonfond, B., Grodent, D., & Radioti, A. (2011). Improved mapping of Jupiter's auroral features to magnetospheric sources. *Journal of Geophysical Research: Space Physics*, *116*(A3). doi: 10.1029/2010JA016148